

Article

Investigation of the Tribological Properties of Different Textured Lead Bronze Coatings under Severe Load Conditions

Adolfo Senatore ¹, Giacomo Risitano ², Lorenzo Scappaticci ³ and Danilo D'Andrea ^{2,*}

¹ Department of Industrial Engineering, University of Salerno, Via Giovanni Paolo II, 132, 84084 Fisciano, SA, Italy; a.senatore@unisa.it

² Department of Engineering, University of Messina, Contrada di Dio (S. Agata), 98166 Messina, SA, Italy; grisitano@unime.it

³ Sustainability Engineering Department, Guglielmo Marconi University, via Plinio 44, 00193 Rome, SA, Italy; l.scappaticci@unimarconi.it

* Correspondence: dandread@unime.it; Tel.: +39-393-020-9246

Abstract: The purpose of this paper is to investigate the variation in the coefficient of friction (CoF) and also the wear in a lead bronze coating under different texture conditions. The tribological tests were performed using a tribometer with pin on disk configuration. Several kinds of textures, realised by a surface laser texturing, were tested by varying the diameter, depth, and density of the dimples under severe working conditions. The innovative aspect concerns the behaviour of the textured lead bronze coating and the lubrication conditions when the sample is subjected to extreme load conditions. Confocal microscopies and SEM (Scanning Electron Microscopy)/EDS (Energy Dispersive X-Ray Spectroscopy) analyses were performed to evaluate the texture behaviour and also the surface deterioration of the coating. The results show that the application of texture processing leads to an improvement in the tribological properties of the coating. By analysing separately the variation of the different geometric parameters of the dimples, it has been shown that the best results are obtained with a diameter of 50 μm , a density of 5%, and a depth of 5 μm .

Keywords: laser surface texturing; wear; friction



Citation: Senatore, A.; Risitano, G.; Scappaticci, L.; D'Andrea, D. Investigation of the Tribological Properties of Different Textured Lead Bronze Coatings under Severe Load Conditions. *Lubricants* **2021**, *9*, 34. <https://doi.org/10.3390/lubricants9040034>

Received: 27 February 2021

Accepted: 22 March 2021

Published: 26 March 2021

Publisher's Note: MDPI stays neutral with regard to jurisdictional claims in published maps and institutional affiliations.



Copyright: © 2021 by the authors. Licensee MDPI, Basel, Switzerland. This article is an open access article distributed under the terms and conditions of the Creative Commons Attribution (CC BY) license (<https://creativecommons.org/licenses/by/4.0/>).

1. Introduction

Mechanical components, and in particular hydraulic components, are often subject to sliding contacts and high contact pressure, which cause several failure modes such as delamination, seizure, noise, vibrations, and fatigue crack due to friction and wear [1–3]. The efficiency improvement in piston pumps and motors is one of the most important goals in the development of these machines [4,5]. A small improvement in pump efficiency in terms of percentage points (%) has a significant impact in terms of noise, efficiency, and reduced consumption in many technologies, such as CVT (Continuously Variable Transmission) power split [6].

The reduction in both friction and wear is very important to ensure high efficiency and extension of the component life. Typically, the problem of friction and wear is dealt with by using lubricants, but in some cases such as a low rotation speed, lubrication is insufficient. For this reason, we use coatings capable of guaranteeing dry lubrication, for example lead bronze [7–9]. However, solid lubricants such as lead are now being decommissioned because of their toxicity.

The increasing request for high efficiency anti-friction coatings from modern industries has pushed researchers towards the development of new technologies, such as PVD-TiN coating [10,11] or a super-hydrophobic/super-oleophobic nanostructured surface [12–14]. Another technology studied to enhance the tribological property of materials is surface texturing. Surface texturing has been known for a long time, as shown by the numerous studies reported in the scientific literature [15–18]. The use of texture to improve the

performance of mechanical systems and reduce friction and wear is particularly used in the automotive field, as demonstrated by numerous scientific studies [19–23]. Borghi et al. [24] have studied the effects of surface modification by laser texturing on tribological performances of nitriding steel for high-performance engine applications. Vladescu et al. [25] have investigated the effect of surface texture on friction for a convergent–divergent bearing, operating under different lubrication regimes. However, almost all the scientific works analysed investigate the tribological behaviour of texturing subjected to loads varying between 5 and 100 N [26–28].

The novelty of this paper is the use of extremal working condition to analyse the applications of surface texturing on hydraulic pumps and motors, which represent some of the components most studied for the application of this technology [29–32]. Another innovative aspect is the use of surface texturing on a lead bronze alloy, which already has anti-friction characteristics.

To reduce friction and wear, different shapes of texture can be used, such as dimples, holes, cavities or asperities, but the most used is the micro-dimples; moreover, the effect of the spatial arrangement of the dimples could be evaluated. There are many techniques to achieve surface texturing including etchant, ion beam texturing, embossing, and laser surface texturing (LST), which is the most applied technique [33] and has been used in this work.

Texturised surfaces have numerous advantages in terms of mechanical and tribological behaviour. In fact, the presence of micro-incisions, allows an improvement of the tribological behavior in the case of starved lubrication, as the dimples act as oil reservoir [34]. While, in the case of hydrodynamic or mixed lubrication, the micro-dimples behave like hydrodynamic bearings [35]. Another important feature of texturised surfaces is the ability to reduce abrasive wear, as micro-engravings behave like traps for debris.

In this paper different types of textures were tested, varying the diameter, depth, and density of the dimples, using the pin on disk technique. After the tribological tests, failure analysis was performed in order to evaluate the impact of the texture on the lead bronze coating.

2. Materials and Methods

The tribological tests were performed by using reciprocating tester. The tribo-system consists of the stationary sample (counter-specimen) pressed at the required load against the cylinder sample (specimen) performing reciprocating motion. The coefficients of friction and wear were calculated using a UMT-3 tribometer in the configuration pin-on-disc (CETR Ltd., USA), according to ASTM G99-05 (2010). A cylinder pin (Figure 1a) of 100Cr6Steel (diameter 6.0 mm, length 20.0 mm) is placed in contact with a known and regulated vertical load (constant) on the surface of the discs (a 70.0 mm diameter with a bronze thickness of 0.8 mm) (Figure 1b). From the measurement of the lateral force, it is possible to obtain the coefficient of friction by the ratio between the lateral and vertical force.

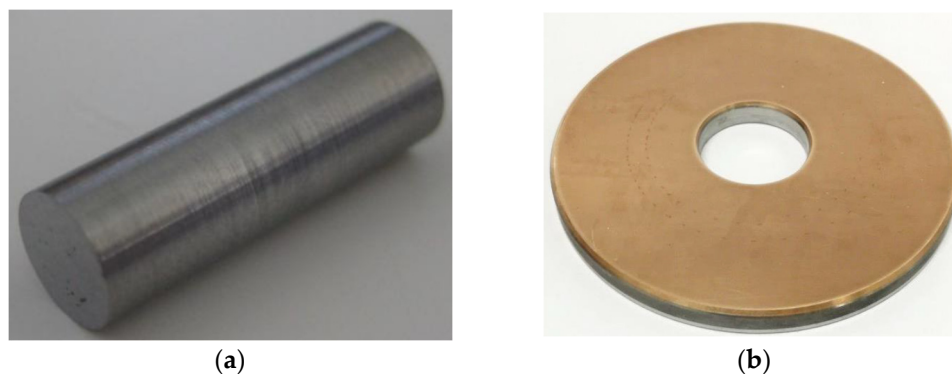


Figure 1. (a) The cylinder pin of a Steel 100Cr6 (b) bi-metal disk.

The tribometer is shown in Figure 2.

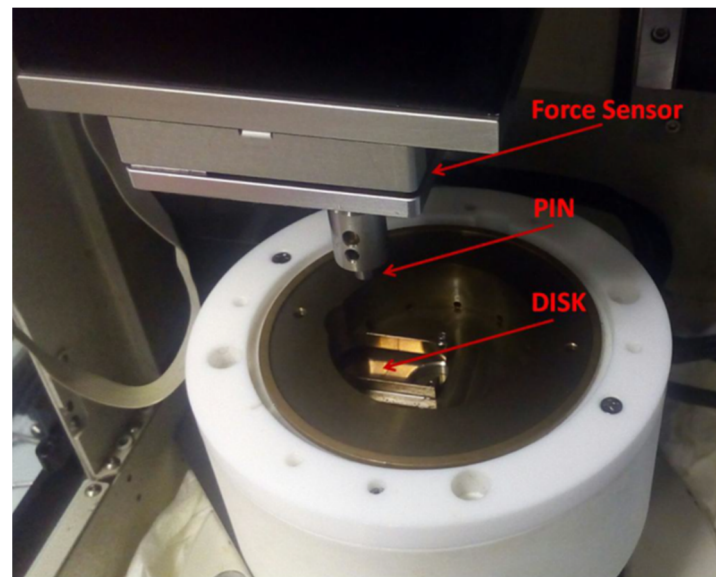


Figure 2. Tribometer system (CETR UMT-3).

The tribological tests have been performed with specimens fully immersed in the lubricant bath. The oil lubricant used was LI-HIV 46 (viscosity index 175). It is used in hydraulics machines, such as pumps and motors. Table 1 shows the characteristics of the lubricating oil.

Table 1. LI-HIV 46 oil parameters.

| Parameters | Value |
|---------------------|----------------------|
| Density at 20 °C | 46 kg/m ³ |
| Viscosity at 40 °C | 46 cSt |
| Viscosity at 100 °C | 9 cSt |
| Viscosity Index | 175 |
| Freezing °C | −35 |
| Flammability °C | 210 |

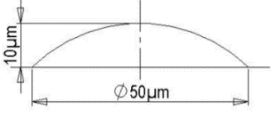
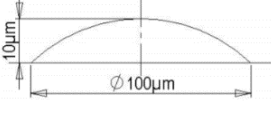
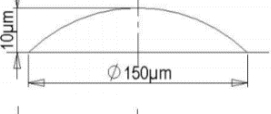
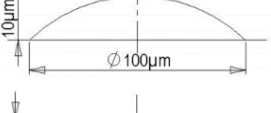
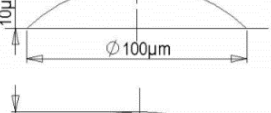
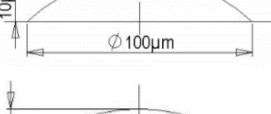
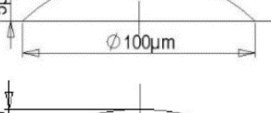
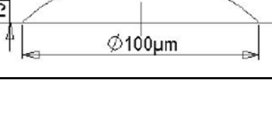
The temperature system is composed by a thermocouple immersed in the oil bath. The test parameters are shown in Table 2.

Table 2. Tribological test parameters.

| Parameters | Value |
|------------------|----------|
| Vertical load | 706.8 N |
| Contact pressure | 25 MPa |
| Rotation speed | 2000 rpm |
| Oil temperature | ≅ 70 °C |
| Time | 10 min |
| Lubrication | full |

The micro-structured surface on bi-metal cylinder disk samples have been realised using surface laser texturing technique. Nine typologies of texture, varying diameter, depth, and density of the dimples on the surface have been produced. The features of the different kind of samples are reported in Table 3.

Table 3. Information of texture parameters.

| Sample Name | Typology of Texture | Density Area (mm ²) |
|-------------|--|--|
| A | As produced | Not considered |
| B50 |  | 10% of total area (334.8 mm ²) |
| B100 |  | 10% of total area (334.8 mm ²) |
| B150 |  | 10% of total area (334.8 mm ²) |
| C5 |  | 5% of total area (167.4 mm ²) |
| C15 |  | 15% of total area (502.2 mm ²) |
| C20 |  | 20% of total area (669.6 mm ²) |
| D5 |  | 10% of total area (334.8 mm ²) |
| D15 |  | 10% of total area (334.8 mm ²) |

In total, 36 samples were realised; they can be classified in four classes labelled with the letters A, B, C, D. As shown in Table 3, the samples A is “as produced”, without any kind of texture; the samples in B (Figure 3a–c) were produced by changing the diameter of the dimples, keeping a fixed depth and density of dimples; the samples in C (Figure 4a–c) were made by changing the density, keeping an unchanged depth and diameter of dimples. The latter kind of samples in D (Figure 5a,b) were produced by changing only the depth of the dimples. The surface laser texturing was carried out on lead bronze specimens (EN CC496K). This material is typically used for anti-friction coating in the hydraulic industry. In this case, it is used as a coating for valve plates and cylinder blocks in axial piston pumps.

A failure analysis was performed to characterise the influence of the dimples and the microstructure of the bronze alloy subjected to the tribological test through the use of an optical microscope (OM), a scanning electronic microscope (SEM) equipped with an EDS probe, and a confocal microscope. The optical microscopy was carried out by means of a LEICA stereomicroscope (LEICA Microsystems GmbH, Wetzlar, Germany), while the SEM microscopy was carried out by TM3030PLUS (HITACHI, Tokyo, Japan). Confocal microscopies (Leica DCM 3D) were performed with a 100× lens whose characteristics are shown in the Table 4.

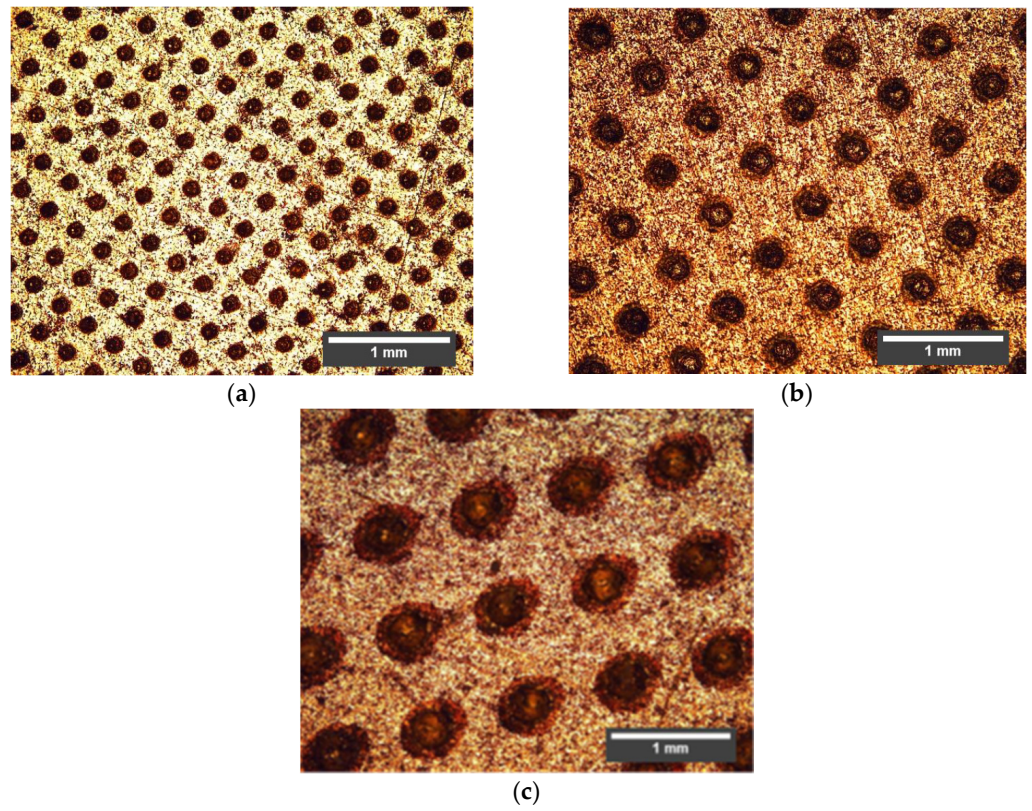


Figure 3. (a) B50 sample, (b) B100 sample, (c) B150 sample.

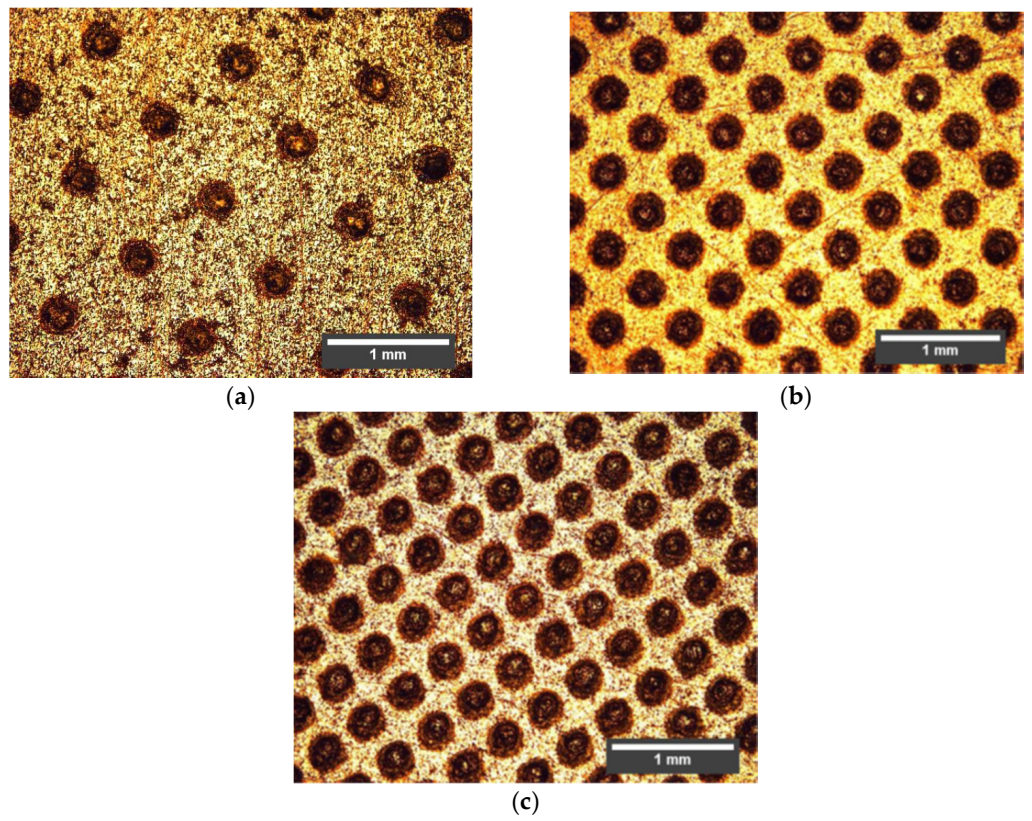


Figure 4. (a) C5 sample, (b) C15 sample, (c) C20 sample.

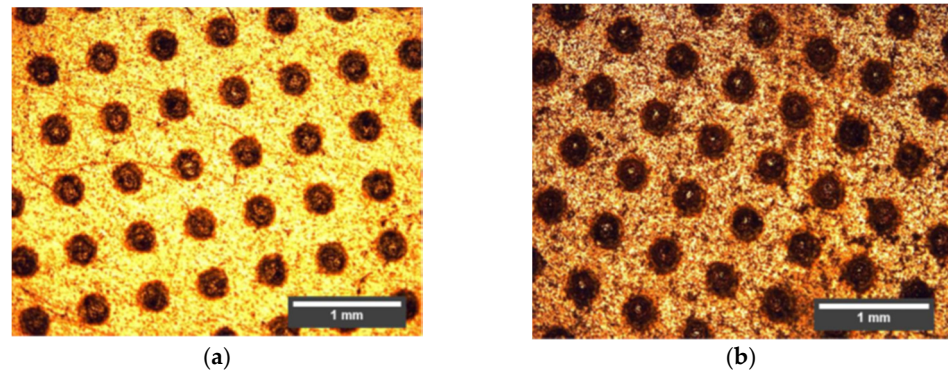


Figure 5. (a) D5 sample, (b) D15 sample.

Table 4. Characteristic parameters of the 100× lens.

| Characteristic Parameters | | | | |
|---------------------------|-------------------------|-----------------------|------------------------------|------------------------------|
| Objective | NA (Numerical Aperture) | WD (Working Distance) | Pixel Size (μm) | Min. Range (μm) |
| 100× | 0.9 | 0.27 | 0.16 | 4 |

3. Results and Discussion

To evaluate the behavior of the bronze alloy coating subject to texture processing, tribological tests were carried out according to the specifications shown in Table 2. It should be noted that very high loads have been specifically chosen, compared to the loads generally used in the literature, to simulate the severe contact conditions to which the rotating parts of the axial piston pumps are subjected in conditions of poor lubrication.

3.1. Friction and Wear

Figure 6 shows the variation of the friction coefficient as a function of time, while in Table 5 the averages of the friction coefficients are shown.

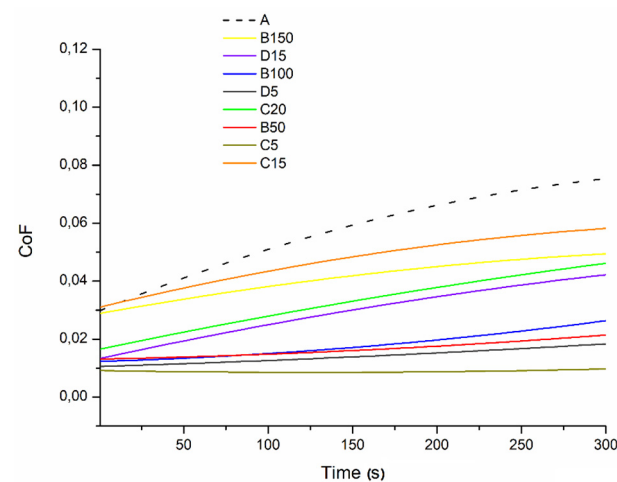


Figure 6. Comparison of the different coefficients of friction.

Table 5. Averages of coefficients of friction.

| Averages of Coefficients of Friction | | | | | | | | |
|--------------------------------------|-------|-------|-------|-------|-------|-------|-------|-------|
| A | B50 | B100 | B150 | C5 | C15 | C20 | D5 | D15 |
| 0.066 | 0.023 | 0.029 | 0.045 | 0.010 | 0.053 | 0.043 | 0.019 | 0.039 |

By analysing the trend of the friction coefficients shown in Figure 6, it is possible to notice that the non-textured specimen maintains a higher friction coefficient compared to the textured samples when subjected to a load of 706.8 N. The friction coefficient decreases by producing the dimples on the surface of the samples; however, by changing the characteristics of the texture, the response of the coating in terms of friction coefficient also changes, which does not always represent an improvement compared to the non-textured surface. In fact, Figure 6 shows that at the end of the test for some types of profiles, the friction coefficient increases reaching values similar to the unprocessed specimen. As highlighted by the values shown in Table 5, sample C5 maintains an average COF of 0.010, which remains constant for almost the entire tribological test and represents a net improvement in the tribological behaviour when compared with the untextured sample A, which shows an average value of the COF equal to 0.066. An interesting analysis regards the influence assumed by the variation of a single geometric parameter on the friction coefficient.

3.2. Effect of Dimples Diameter

Figure 7 shows the trend of the friction coefficient as a variation of the diameter of the dimples.

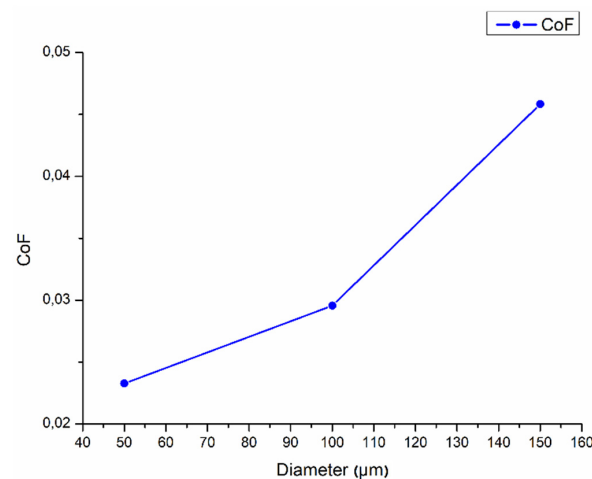


Figure 7. Variation of the friction coefficient as a function of the diameter of dimples.

The curve shows that as the diameter of the dimples increases, the friction coefficient increases [36]. This behaviour of the coating may be due in part to the formation of pile-up, i.e., the accumulations of bronze alloy due to the melting generated by the processing of laser texturing (Figure 8).

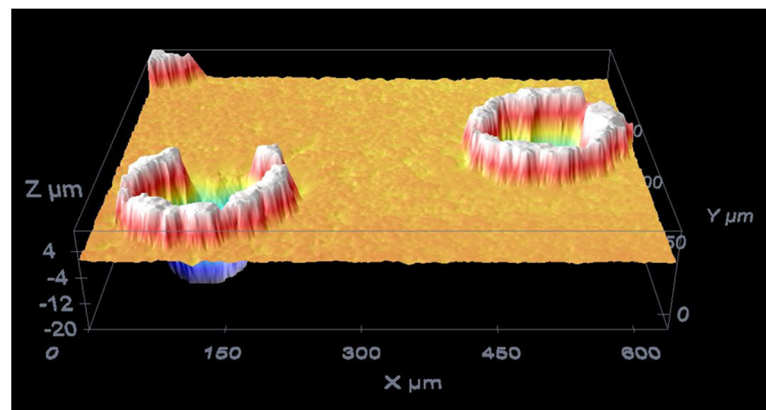


Figure 8. Confocal analysis of the surface of sample B150, which highlights the presence of pile-up.

The greater the dimples diameter, the greater the height of the pile-up, and therefore the greater the friction generated on contact with the counter-specimen. In fact, Figure 9 shows the profile of the surface along the x axis. It is possible to notice that the pile-up assumes dimensions of even 20 μm .

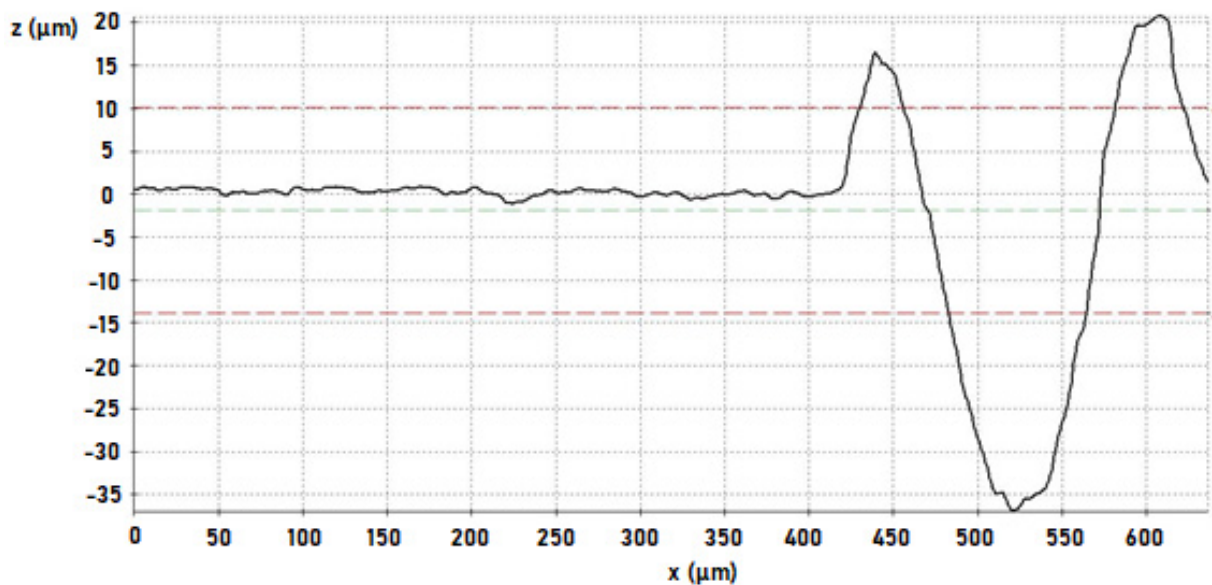


Figure 9. Profile analysis of specimen B150.

The increase in friction coefficients can also be explained by the decrease in lubrication during the test. In fact, by increasing the size of the dimples, the oleophobicity of the coating decreases and the oil remains trapped inside the dimples. By comparing the wear track in the case of specimen B50 and in the case of specimen B150 (Figure 10a,b), it can be underlined that in the second case an evident phenomenon of seizure was generated in part due to poor lubrication, and in part due to the formation of debris, favoured by the presence of pile-up as highlighted by the SEM analyses in Figure 11.

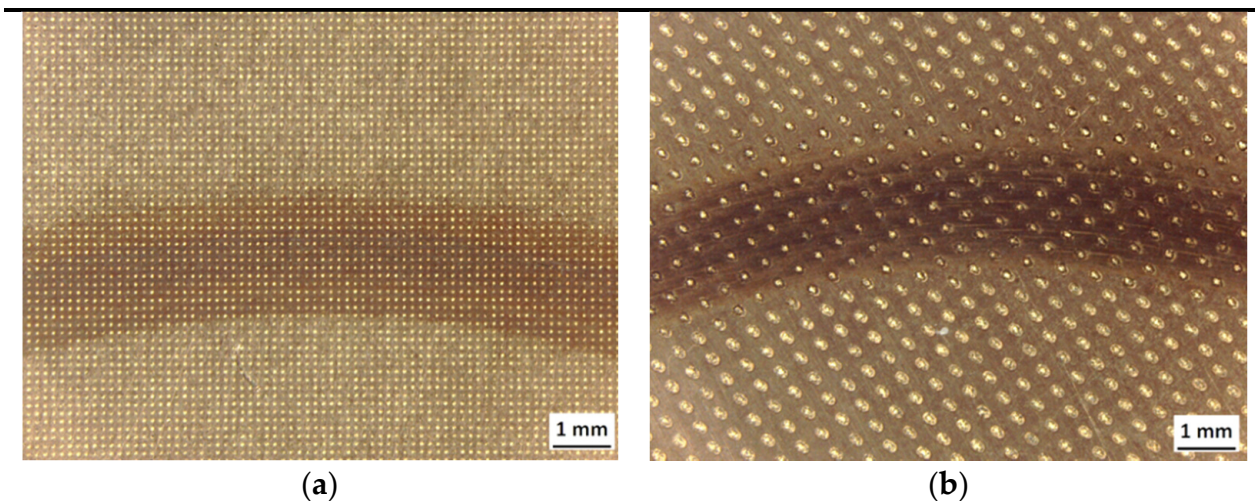


Figure 10. (a) Wear track of sample B50, (b) wear track of sample B150.

Since the bronze alloy is very malleable, the pile-up in contact with the pin (100Cr6) is partially removed with the formation of debris and partially “spread” on the dimples causing a partial occlusion.

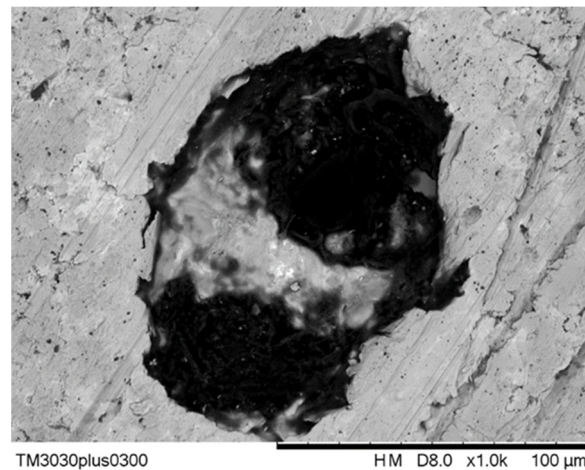


Figure 11. The SEM image shows the presence of bronze alloy debris inside the dimples.

3.3. Effect of Dimples Density

Figure 12 shows the trend of the friction coefficient as a variation of the density of dimples.

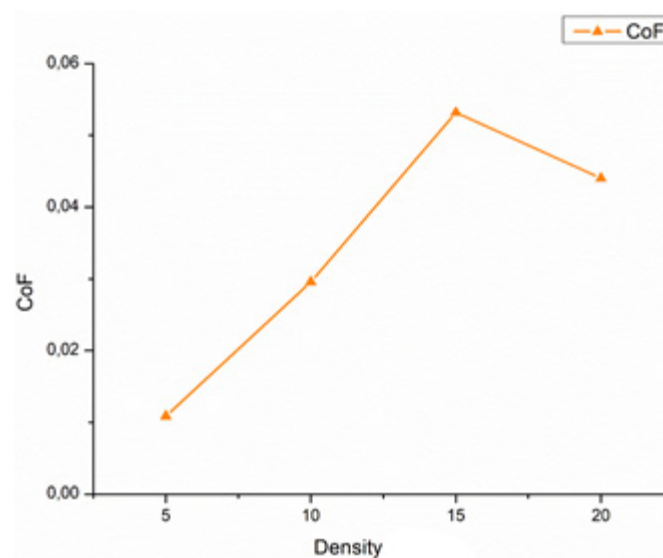


Figure 12. Variation of the friction coefficient as a function of the density of dimples.

As shown by the trend of the orange curve in Figure 12, by varying the density of the dimples on the surface of the sample, the friction coefficient also varies. The effect shown by the tribological tests is unexpected with respect to the predicted trend of the coefficient of friction (CoF). As the area of the surface occupied by the dimples increases, a decrease in CoF is expected due to the increase in the surface oleophobicity; i.e., the contact angle increases as the surface roughness increases. This observation is partly true, but as demonstrated also by [18] et al., the increase in density can lead to an increase in the friction coefficient due to an increase in roughness and to the pile-up, whose increase is proportional to the quantity of dimples present on the surface. What can be noticed is that the parameter Sa (Table 6), which represents the average roughness of the analysed surface, increases with the density of the dimples. In particular, for the C5 specimen with a density of 5% there will be an average roughness Sa equal to 1.08 μm ; for the C15 specimen with a density of 15% there will be an average roughness Sa equal to 2.13 μm ; for the C20 specimen with a density of 20% there will be an average roughness Sa equal to 2.50 μm .

Table 6. Surface parameters obtained with confocal microscopy of an area of $636 \times 427 \mu\text{m}^2$ with a resolution of $10^{-4} \mu\text{m}$.

| Name | Characteristic Parameters | |
|------|---------------------------|--------------------|
| | Max | Sa |
| C5 | 8.4017 μm | 1.08 μm |
| C15 | 8.3067 μm | 2.13 μm |
| C20 | 10.582 μm | 2.50 μm |

The surface deterioration due to the tribological test is evident by analysing Figure 13a,b which show the confocal scans of the C20 specimen before and after the test.

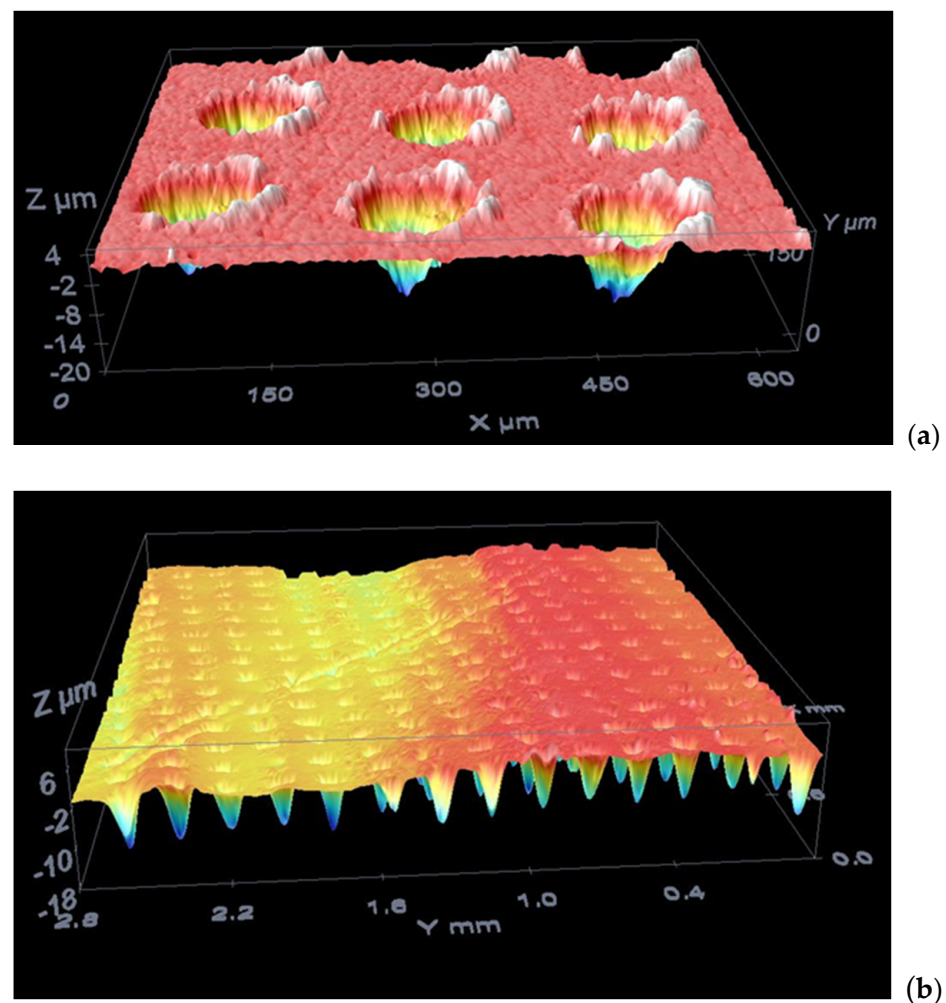


Figure 13. (a) Confocal scan of C20 specimen untested surface; (b) confocal scan of C20 specimen after the tribological test.

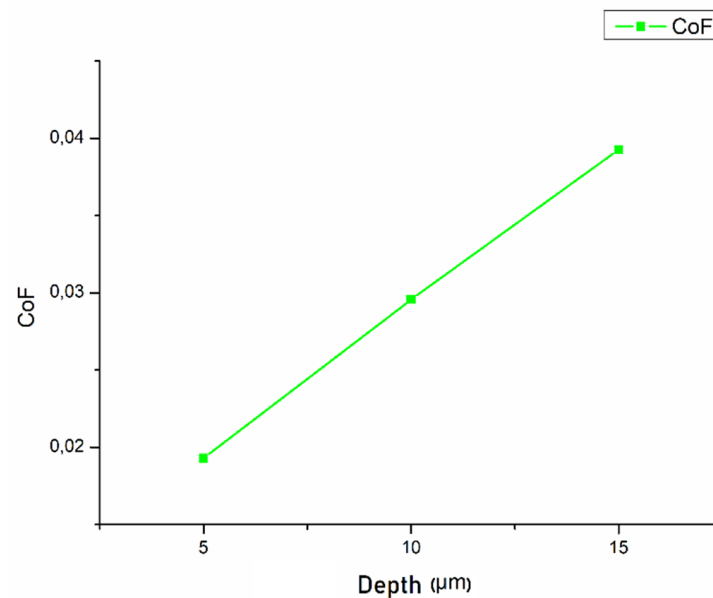
From Figure 13b it can be detected that on the wear track there are microgrooves, which indicate the presence of abrasive particles. In Figure 13a, the pile-ups are instead very evident, highlighted in white in the image. A more detailed analysis of the wear track was carried out with the SEM microscope and the EDS probe. In Table 7 the values calculated according to ISO 25178 are reported. The mean values of the roughness of untested and tested specimens are, respectively, 2.68 μm and 1.65 μm .

Table 7. Summary of roughness parameters.

| Parameter | Height Parameters | |
|-----------------------|-------------------|--------|
| | Untested | Tested |
| Sq (μm) | 3.70 | 3.13 |
| Ssk (μm) | −1.42 | −3.03 |
| Sku (μm) | 5.68 | 12.70 |
| Sp (μm) | 10.38 | 10.05 |
| Sv (μm) | 20.65 | 18.33 |
| Sz (μm) | 31.04 | 28.38 |
| Sa (μm) | 2.68 | 1.65 |

3.4. Effect of Dimple Depth

Figure 14 shows the trend of the friction coefficient as a variation of the depth of the dimples.

**Figure 14.** Variation of the friction coefficient as a function of the depth of the dimples.

It is possible to highlight in Figure 14 the friction coefficient increases with increasing depth of the dimples [37]. This behaviour could be due to an excessive “reservoir” effect of the dimples, which with increasing depth tend to catch the oil and do not allow correct lubrication. Additionally, in this case, the increase in the depth of the dimples could lead to a decrease in the surface oleophobicity and therefore a poor lubrication. After separately analysing the effect of the diameter, density, and depth of the dimples on the friction coefficient, it is possible to confirm that a lower density associated with a lower depth provides a visible improvement on the friction coefficient compared to the change in diameter.

3.5. Wear Track

As mentioned in the previous paragraphs, the presence of the pile-up can trigger abrasive wear, as shown by the microgrooves in Figure 13b (previous paragraph). To analyse the state of the wear track in more detail, microscopies were performed with the aid of the SEM. The B150 was chosen as the specimen to be studied, as shown in Figure 15, in which the diameter of the dimples is measured, which is around 150 μm , as per specifications in Table 3.

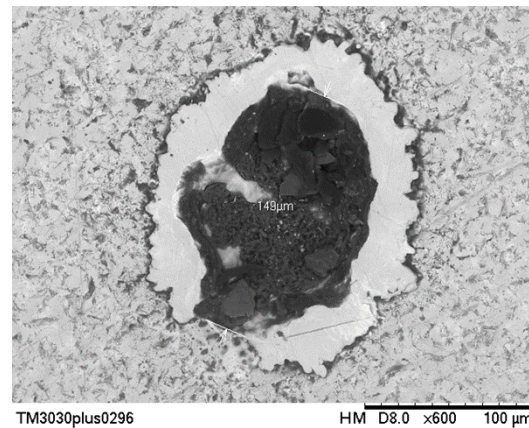


Figure 15. SEM image at 600× of the dimple of the B150 specimen.

Analysing the wear track (Figure 16), one should note the presence of the microgrooves due to the action of an abrasive particle, which could be associated to the action of debris that was formed by detachment of a portion of pile-up, or it could be debris due to pin deterioration.

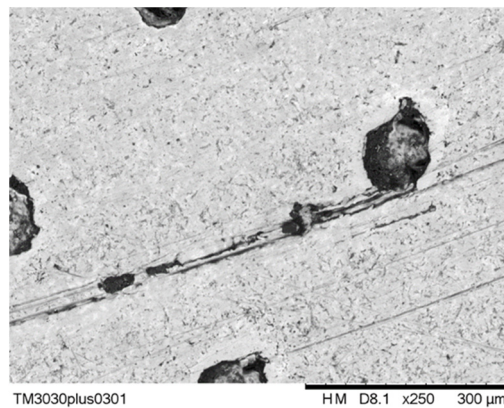


Figure 16. SEM image at 250× of microgrooves on a bronze alloy surface.

To confirm the composition of the debris, a “point and shot” analysis with the EDS probe was performed. As can be seen in Figure 17, the analysis of the debris returns the characteristic peak of Fe at 6.4 keV. Since there is no iron presence in the composition of the bronze alloy, the particles that generated the microgrooves certainly come from the pin deterioration.

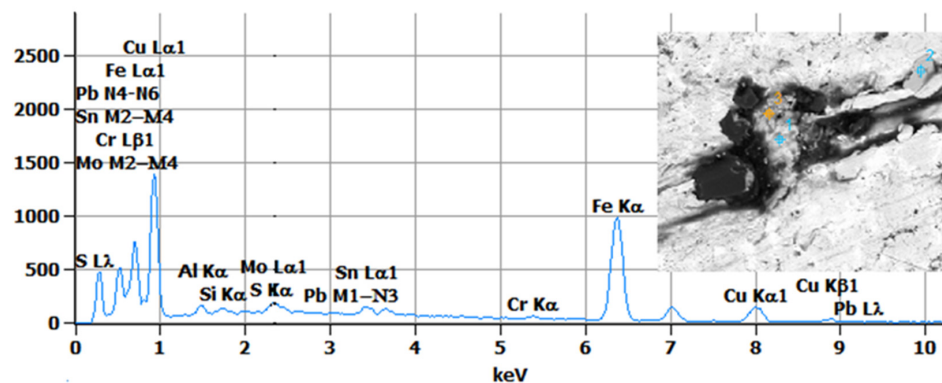


Figure 17. EDS analysis shows the presence of Fe through the characteristic peak at 6.4 keV.

4. Conclusions

In order to increase the efficiency of components that work under reciprocating sliding, the application of the surface texture on an antifriction coating used in the automotive and hydraulic fields was tested. By using a low economic impact technique such as surface laser texturing, it is possible to decrease the friction coefficient of a surface and at the same time increase the oleophobicity and therefore improve lubrication, especially in starved lubrication conditions. The improvement in lubrication due to surface texturing influenced the COF value which remained low for almost all types of textures, even under extreme load conditions. The study was carried out on a lead bronze alloy which, owing to the lubricating characteristics of lead, maintains a low friction coefficient. Three types of specimens were tested by varying the geometric characteristics of the dimples, i.e., diameter (class B), density (class C), and depth (class D). It has been demonstrated that by decreasing the diameter of the dimples, the CoF also decreased. Additionally, by increasing the depth of the dimples, the CoF increases. On the other hand, increasing the surface density of the dimples increases the CoF. The results obtained are very interesting and show how the application of the surface texture affects the decrease in the friction coefficient, which assumes a lower value for all textured samples than untextured, which demonstrates how the alloy used already has high anti-friction properties due to the presence of lead which acts as a solid lubricant. The future challenge is to eliminate lead from the bronze alloy, due to its toxicity, and to use the texture to keep the friction coefficient low.

Author Contributions: Conceptualization, G.R. and L.S.; methodology, D.D. and A.S.; validation, G.R., L.S. and A.S.; formal analysis, D.D.; investigation, D.D.; data curation, D.D.; writing—original draft preparation, D.D.; writing—review and editing, D.D. and A.S.; visualization, D.D. and A.S.; supervision, G.R. and L.S. All authors have read and agreed to the published version of the manuscript.

Funding: The author(s) received no financial support for the research, authorship, and/or publication of this article.

Data Availability Statement: The data presented in this study are available on request from the corresponding author.

Conflicts of Interest: The authors declared no potential conflicts of interest with respect to the research, authorship, and/or publication of this article.

References

1. D'Andrea, D.; Epasto, G.; Bonanno, A.; Guglielmino, E.; Benazzi, G. Failure analysis of anti-friction coating for cylinder blocks in axial piston pumps. *Eng. Fail. Anal.* **2019**, *104*, 126–138. [[CrossRef](#)]
2. Ye, S.; Zhang, J.; Xu, B.; Song, W.; Chen, L.; Shi, H.; Zhu, S. Experimental and numerical studies on erosion damage in damping holes on the valve plate of an axial piston pump. *J. Mech. Sci. Technol.* **2017**, *31*, 4285–4295. [[CrossRef](#)]
3. Xu, L.; Sun, H.; Xu, S. Fracture mechanism analysis on the slipper retainer in axial piston pumps. *Eng. Fail. Anal.* **2017**, *80*, 378–385. [[CrossRef](#)]
4. Achten, P.; Mommers, R.; Stelson, K.; Schmitz, K. Measuring the Losses of Hydrostatic Pumps and Motors. In Proceedings of the ASME/BATH Symposium on Fluid Power and Motion Control, Sarasota, FL, USA, 7–9 October 2019; pp. 1–11.
5. Bergada, J.M.; Davies, D.L.; Kumar, S.; Watton, J. The effect of oil pressure and temperature on barrel film thickness and barrel dynamics of an axial piston pump. *Meccanica* **2012**, *47*, 639–654. [[CrossRef](#)]
6. Rossetti, A.; Macor, A.; Scamperle, M. Optimization of components and layouts of hydromechanical transmissions. *Int. J. Fluid Power* **2017**, *18*, 123–134. [[CrossRef](#)]
7. Kestursatya, M.; Kim, J.K.; Rohatgi, P.K. Wear performance of copper-graphite composite and a leaded copper alloy. *Mater. Sci. Eng. A* **2003**, *339*, 150–158. [[CrossRef](#)]
8. Prasad, B.K.; Patwardhan, A.K.; Yegneswaran, A.H. Factors controlling dry sliding wear behaviour of a leaded tin bronze. *Mater. Sci. Technol.* **1996**, *12*, 427–435. [[CrossRef](#)]
9. Pathak, J.P. Seizure resistance characteristics of Cu–Pb bearing alloys. *Mater. Sci. Technol.* **1993**, *9*, 403–407. [[CrossRef](#)]
10. Hong, Y.-S.; Lee, S.-Y.; Kim, S.-H.; Lim, H.-S. Improvement of the low-speed friction characteristics of a hydraulic piston pump by PVD-coating of TiN. *J. Mech. Sci. Technol.* **2006**, *20*, 358–365. [[CrossRef](#)]
11. Lee, S.Y.; Kim, S.D.; Hong, Y.S. Application of the duplex TiN coatings to improve the tribological properties of Electro Hydrostatic Actuator pump parts. *Surf. Coat. Technol.* **2005**, *193*, 266–271. [[CrossRef](#)]

12. Dyett, B.; Lamb, R. Correlating Material Properties with the Wear Behavior of Sol–Gel Derived Superhydrophobic Films. *Adv. Mater. Interfaces* **2016**, *3*, 1–6. [[CrossRef](#)]
13. Rizzo, G.; Massarotti, G.P.; Bonanno, A.; Paoluzzi, R.; Raimondom, M.; Blosi, M.; Veronesi, F.; Caldarelli, A.; Guarini, G. Axial piston pumps slippers with nanocoated surfaces to reduce friction. *Int. J. Fluid Power* **2015**, *16*, 1–10. [[CrossRef](#)]
14. Fotovvati, B.; Dehghanghadikolaei, A.; Namdari, N. Laser-Assisted coating techniques and surface modifications: A short review. *Part. Sci. Technol.* **2020**, 1–10. [[CrossRef](#)]
15. Kovalchenko, A.; Ajayi, O.; Erdemir, A.; Fenske, G.; Etsion, I. The effect of laser texturing of steel surfaces and speed-load parameters on the transition of lubrication regime from boundary to hydrodynamic. *Tribol. Trans.* **2004**, *47*, 299–307. [[CrossRef](#)]
16. Etsion, I. Improving tribological performance of mechanical components by laser surface texturing. *Tribol. Lett.* **2004**, *17*, 733–737. [[CrossRef](#)]
17. Ronen, A.; Etsion, I.; Kligerman, Y. Friction-reducing surface-texturing in reciprocating automotive components. *Tribol. Trans.* **2001**, *44*, 359–366. [[CrossRef](#)]
18. Shum, P.W.; Zhou, Z.F.; Li, K.Y. Investigation of the tribological properties of the different textured DLC coatings under reciprocating lubricated conditions. *Tribol. Int.* **2013**, *65*, 259–264. [[CrossRef](#)]
19. Guarnaccio, A.; Belviso, C.; Montano, P.; Toschi, F.; Orlando, S.; Ciaccio, G.; Ferreri, S.; Trevisan, D.; Mollica, D.; Parisi, G.P.; et al. Femtosecond laser surface texturing of polypropylene copolymer for automotive paint applications. *Surf. Coat. Technol.* **2021**, *406*, 126727. [[CrossRef](#)]
20. Ryk, G.; Etsion, I. Testing piston rings with partial laser surface texturing for friction reduction. *Wear* **2006**, *261*, 792–796. [[CrossRef](#)]
21. Ryk, G.; Kligerman, Y.; Etsion, I. Experimental investigation of laser surface texturing for reciprocating automotive components. *Tribol. Trans.* **2002**, *45*, 444–449. [[CrossRef](#)]
22. Vlădescu, S.C.; Medina, S.; Olver, A.V.; Pegg, I.G.; Reddyhoff, T. Lubricant film thickness and friction force measurements in a laser surface textured reciprocating line contact simulating the piston ring-liner pairing. *Tribol. Int.* **2016**, *98*, 317–329. [[CrossRef](#)]
23. Andersson, P.; Koskinen, J.; Varjus, S.; Gerbig, Y.; Haefke, H.; Georgiou, S.; Zhmud, B.; Buss, W. Microlubrication effect by laser-textured steel surfaces. *Wear* **2007**, *262*, 369–379. [[CrossRef](#)]
24. Borghi, A.; Gualtieri, E.; Marchetto, D.; Moretti, L.; Valeri, S. Tribological effects of surface texturing on nitriding steel for high-performance engine applications. *Wear* **2008**, *265*, 1046–1051. [[CrossRef](#)]
25. Vlădescu, S.C.; Olver, A.V.; Pegg, I.G.; Reddyhoff, T. The effects of surface texture in reciprocating contacts—An experimental study. *Tribol. Int.* **2015**, *82*, 28–42. [[CrossRef](#)]
26. Wang, X.; Liu, W.; Zhou, F.; Zhu, D. Preliminary investigation of the effect of dimple size on friction in line contacts. *Tribol. Int.* **2009**, *42*, 1118–1123. [[CrossRef](#)]
27. Petterson, U.; Jacobson, S. Friction and wear properties of micro textured DLC coated surfaces in boundary lubricated sliding. *Tribol. Lett.* **2004**, *17*, 553–559. [[CrossRef](#)]
28. Kovalchenko, A.; Ajayi, O.; Erdemir, A.; Fenske, G. Friction and wear behavior of laser textured surface under lubricated initial point contact. *Wear* **2011**, *271*, 1719–1725. [[CrossRef](#)]
29. Zhu, Y.; Chen, X.; Zou, J.; Yang, H. A study on the influence of surface topography on the low-speed tribological performance of port plates in axial piston pumps. *Wear* **2015**, 338–339, 406–417. [[CrossRef](#)]
30. Wang, Z.; Gu, L.; Li, L. Experimental studies on the overall efficiency performance of axial piston motor with a laser surface textured valve plate. *Proc. Inst. Mech. Eng. Part B J. Eng. Manuf.* **2013**, *227*, 1049–1056. [[CrossRef](#)]
31. Petterson, U.; Jacobson, S. Textured surfaces for improved lubrication at high pressure and low sliding speed of roller/piston in hydraulic motors. *Tribol. Int.* **2007**, *40*, 355–359. [[CrossRef](#)]
32. Wang, Z.; Hu, S.; Zhang, H.; Ji, H.; Yang, J.; Liang, W. Effect of surface texturing parameters on the lubrication characteristics of an axial piston pump valve plate. *Lubricants* **2018**, *6*, 49. [[CrossRef](#)]
33. Grabon, W.; Koszela, W.; Pawlus, P.; Ochwat, S. Improving tribological behaviour of piston ring-cylinder liner frictional pair by liner surface texturing. *Tribol. Int.* **2013**, *61*, 102–108. [[CrossRef](#)]
34. Rosén, B.-G.; Nilsson, B.; Thomas, T.R.; Wiklund, D.; Xiao, L. Oil pockets and surface topography: Mechanisms of friction reduction. In Proceedings of the XI. International Colloquium on Surfaces, Chemnitz, Germany, 2–3 February 2004.
35. Costa, H.L.; Hutchings, I.M. Hydrodynamic lubrication of textured steel surfaces under reciprocating sliding conditions. *Tribol. Int.* **2007**, *40*, 1227–1238. [[CrossRef](#)]
36. Kasem, H.; Stav, O.; Grützmacher, P.; Gachot, C. Effect of low depth surface texturing on friction reduction in lubricated sliding contact. *Lubricants* **2018**, *6*, 62. [[CrossRef](#)]
37. Tauviqirrahman, M.; Jamari, J.; Wibowo, B.S.; Fauzan, H.M.; Muchammad, M. Multiphase Computational Fluid Dynamics Analysis of Hydrodynamic Journal Bearing Under the Combined Influence of Texture and Slip. *Lubricants* **2019**, *7*, 97. [[CrossRef](#)]